7.5 A Dual Ion Irradiation Study of Helium-DPA Interactions on Cavity Evolution in Tempered Martensitic Steels and Nanostructured Ferritic Alloys — T. Yamamoto, Y. Wu, G. Robert Odette (University of California Santa Barbara), K. Yabuuchi, S. Kondo, and A. Kimura (Kyoto University)

OBJECTIVE

The objective of the research is to find how cavity and other evolutions are influenced by the starting microstructure and irradiation variables, including, displacements per atom (dpa), dpa rate, He/dpa ratio. This particular report is to give an extended summary of our recently accepted publication in Journal of Nuclear Materials.

SUMMARY

Cavity evolutions in a normalized and tempered martensitic steel (TMS) and two nanostructured ferritic alloys (NFA) under Fe^{3+} and He^{+} dual ion beam irradiations (DII) at 500°C and 650°C were characterized over a wide range of dpa, He and He/dpa. Transmission electron microscopy (TEM) showed that DII of a 8Cr TMS, at 500°C to up to 60 dpa and 2100 appm He, produced a moderate density of non-uniformly distributed cavities with bimodal sizes ranging from ≈ 1 nm He bubbles to ≈ 20 nm faceted voids, and swelling ≈ 0.44%. In contrast, the same irradiation conditions produced only small ≈ 1.3 nm diameter bubbles and swelling of ≈ 0.05% in the NFA MA957. Similar bubble distributions were observed in MA957 and a developmental NFA DII at 650°C up to ≈ 80 dpa and ≈ 3900 appm He. These results demonstrate the outstanding He management capability of the oxide nano-features in the NFA. The various data trends are shown as a function of dpa, He, He/dpa and He*dpa.

BACKGROUND

Predicting and mitigating the effects of a combination of large levels of transmutant He and displacement damage (dpa), produced by high energy neutrons, on the dimensional stability and mechanical properties of structural materials is one of the key challenges in the development of fusion energy [1]. The fundamental overriding questions about He and dpa effects and their synergisms include: a) what are the basic interacting mechanisms controlling He and displacement defect transport, fate and consequences; b) how are the resulting cavity and other evolutions are influenced by the starting microstructure and irradiation variables, including, displacements per atom (dpa), dpa rate, He/dpa ratio and irradiation temperature; and, c) how can the detrimental effects of He-dpa synergisms be mitigated and managed by proper microstructural designs?

We have previously demonstrated that in situ He implantation (ISHI) in mixed spectrum fission reactor irradiations provides a very attractive approach to assessing the effects of He-dpa synergisms, while avoiding most of the confounding effects associated with Ni- or B-alloy doping type experiments [1-8]. Another approach is to use dual ion beam irradiations (DII) to simultaneously implant He and create displacement damage [1,9-12]. Note, the two techniques are complementary but manifest many differences that, in the case of DII, include: a) much higher dpa rates; b) non-uniform spatial distributions of dpa and He; and, c) the proximity of a free surface. Here we focus on DII encompassing a wide

range of dpa, He and He/dpa that naturally arise from varying profiles of these damage parameters with depth from the specimen surface. Comparisons of DII and ISHI experiments will be the subject of future publications.

Experimental Procedure

The alloys studied here were TMS F82H mod.3 and two NFAs, MA957 and developmental variant 14YWT-PM2 (hereafter referred to as PM2). The mod.3 variant adjusted the base composition of a large program heat F82H-IEA (nominal in wt.%, 7.5Cr 2W 0.2V 0.1C 0.1Si 0.02Ta, 60ppm N, bal. Fe) by reducing the N and Ti to 14 ppm and 0.001%, respectively, while increasing Ta to 0.1% [13]. MA957 is a widely studied representative reference variant of NFA that was first produced by INCO in the late 1970s [5]. The composition of the MA957 heat studied here is 13.6Cr, 0.30Mo, 0.98Ti, 0.26Y_2O_3, balance trace impurities and Fe. NFA are of growing interest due to their radiation damage resistance, and especially their transformational He management capabilities [3,5,6,14]. The average grain size (d_g) in MA 957 is about 0.6 and 1.5 mm in the transverse and axial directions, respectively. Prototypic number densities (N) and average diameter (<d>) of the oxide NFs in MA957 are ≈ $5.6x10^{23}/m^3$ and 2.7 nm, respectively [15]. The corresponding dislocation densities (r) are ≈ $0.8x10^{15}/m^2$. The nominal composition of PM2 is Fe-14%Cr, 3%W, 0.35%Ti, 0.3%Y_2O_3 wt.%, bal. trace impurities and Fe). PM2 was processed at ORNL by D. Hoelzer, as part of a LANL-ORNL-UCSB collaboration to develop larger quantities of best practice NFA [16]. The N, <d>, d_g and r in PM2 are ≈ $8.6x10^{23}/m^3$, 2.1 nm, 424 nm and $1.2x10^{15}/m^2$, respectively [16]. More details about these materials, including processing paths, micro-nanostructures and properties, are given elsewhere [5,13-19].

In the case of the 500°C studies, DII were carried out on 3 mm diameter disks, mechanically ground to a nominal thickness of 200 mm prior to electro-polishishing; the corresponding specimens used in the 650°C study were 500 mm thick 4x8 mm^2 electro-polished coupons. The DII were performed in DuET facility located at the Institute of Advanced Energy, Kyoto University in Japan. Here, Fe^{3+} and He^+ ions are accelerated to 6.4MeV and 1MeV, respectively [20]. The two 500°C irradiations targeted nominal damage levels of 10 dpa/480 appm He and 26 dpa/1200 appm He, respectively, at a reference point 600 nm from the specimen surface. The 650°C irradiation targeted a corresponding 600 nm depth nominal damage level of 48 dpa/2200 appm. Taking advantages of spatial distributions of damage and He concentration produced by the ion irradiations, we analyzed microstructures of the specimens at various He – dpa conditions as shown in Figure 1. The damage calculations are based on the Kinchin-Pease damage energy model, with a displacement energy of 40 eV for Fe and Cr, as recommended in ASTM E521-96 (2009) [21,22]. DuET irradiations provide a basis to evaluate the effects of a wide range of irradiation variables, including high dpa with no He, as well as undamaged regions. Figure 1 shows a corresponding He-dpa map. Damage region in the analyses were selected avoiding the effects of surface proximity and injected self-interstitials. TEM was performed on the FEI 200 keV Technai T20 and 300 KeV Titan instruments in the UCSB Microstructure and Microanalysis Facility. Through focus bright field imaging was used to characterize the cavities.

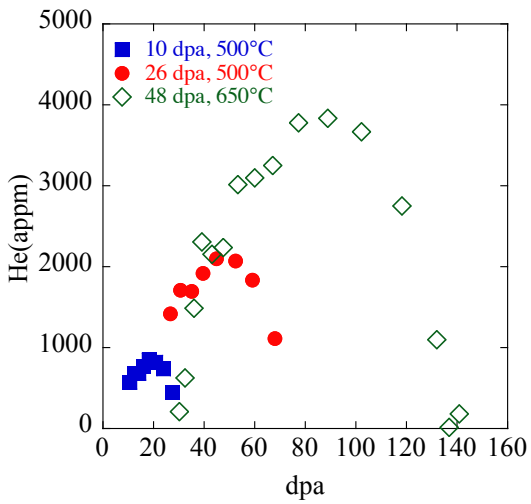

Figure 1. dpa-He conditions in the discrete depth sections where quantitative analyses were carried out.

Key Results

Table 1 briefly summarizes the observed trends in the number density (N), average diameter (<d>) and the volume fraction (f) of cavities in F82H mod.3 (note, trying to describe these complex trends in words quickly becomes very confusing). Some key observations include:

- None of the damage parameters is, in itself, sufficient to represent the data.
- A significant amount of the apparent scatter is also associated with differences in the local alloy microstructure.
- N depends only weakly on, or is independent of, all the damage parameters within the observed scatter.
- <d> systematically increases with He, dpa (with possible peaks) and He*dpa for a given irradiation condition.
- <d> also increases between the lower and higher dpa condition.
- f systematically increases with He, dpa (with possible peaks) and He*dpa for a given irradiation condition.
- f also increases between the lower and higher dpa condition.
- The He*dpa damage parameter provides the most effective correlation with the f trends.

Note, there is no special physical significance to the use of the He*dpa damage parameter, except that both He and dpa are needed for void formation. However, to some extent this parameter captures the critical bubble to void conversion mechanism leading to an incubation dose in void swelling [1,26,27]. This is illustrated in Figure 2a plotting the volume fraction of cavities larger than 4 nm as a function of dpa for various He/dpa ratios. Figure 2b shows the corresponding variation in the number density of the larger cavities. While the absolute swelling and swelling rates are still low, it is important to emphasize that it is likely that the cavity volume fraction will continue to increase in F82H mod.3, and even accelerate at higher dpa, perhaps reaching the nominal 0.2%/dpa proposed by Garner [28].

Table 1. Summary of cavity parameters trends with irradiation variables

N, <d>, f	He	dpa	He/dpa	He*dpa
N	Weak decrease especially at higher dpa	Weak increase at higher dpa	No significant systematic trend	No significant systematic trend
<d>	Systematic increase	Increases with possible peaks at both dpa ranges	No significant systematic trend - or weak drop in going from the lower to higher dpa range	Systematic increase
f	Systematic and scattered increase	Systematic and scattered increase or peak following possible threshold	No significant systematic trend - or weak drop in going from the lower to higher dpa range	Systematic increase after possible threshold

In MA957, the trends are very different than in the F82H3. The <d> are remarkably constant, while the N and f actually appear to decrease slightly with increasing He, dpa and He*dpa. The later trend may reflect sample variations, rather than a real physical trend. The N in MA957 are much higher and the <d> much smaller than in F82H. As described in more detail elsewhere [29], the bubbles are essentially all associated with NFs. These results clearly indicate the ability of NFs in NFA to manage high concentrations of He.

Figure 3 summarizes and cross-compares plots of N, <d> and f versus He*dpa for the different alloys and irradiation conditions. Key observations include:

- At 500°C the trends in the TMS F82H mod.3 are markedly different than in the NFA MA957. F82H mod.3 has fewer and larger void cavities that produce more swelling than in the NFA.
- Except for NFA PM2, the N are generally weakly dependent on He*dpa after an initial rise. This PM2 trend is likely a visibility effect.
- The N in NFA is similar to, or slightly larger than, the number density of NFs, as reflected in the larger N (and f) in PM2 versus MA957.
- The <d> are essentially constant for both NFA and both irradiation conditions, while <d> systematically increases in F82H mod.3.
- A corresponding systematic increase in f void (swelling) begins in the TMS beyond He*dpa ≈ $5x10^4$ appm He-dpa due to the presence of growing voids, as signaled by the trend in <d>.
- The bubble f in the NFA gradually increase with He*dpa at 650°C and are higher that at 500°C.

These results clearly demonstrate the superior He management capability of the NFA compared to TMS, which experience swelling at sufficiently high He and dpa.

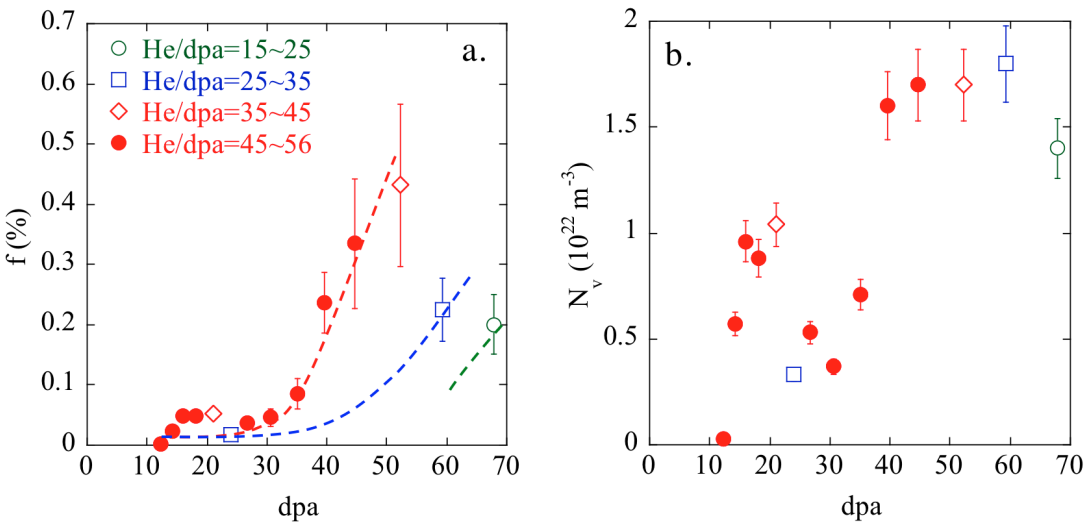

Figure 2. a) The volume fraction, f, and b) number density, N, of cavities larger than 4 nm as a function of the dpa at levels of He/dpa in F82H mod.3 irradiated at 500°C.

SUMMARY

We have summarized the cavity evolutions observed in a TMS and two NFA under Fe^{3+} and He^{+} DII performed at 500°C (F82H mod.3 and MA957) and 650°C (MA957 and PM2), to nominal dpa and He levels of ≈ 10 to 48 dpa and ≈ 480 to 2200 appm, respectively. The TMS F82H mod.3 irradiated at 500°C contains a moderate density of non-uniformly distributed cavities with sizes ranging from ≈ 1 nm (bubbles) up to ≈ 20 nm (voids). In contrast, the MA957 only contains a uniform distribution of small ≈ 1.3 nm diameter bubbles. Notably, qualitatively similar bubble distributions are observed up to ≈ 80 dpa and ≈ 3900 appm He at 650°C, demonstrating the outstanding He management capability of nm-scale features in NFA MA957 and PM2. The observed bubbles are more numerous and the bubble swelling is larger at 650°C compared to 500°C. The total swelling in F82H at 500°C reaches ≈ 0.44% at ≈ 50 dpa, due to a well-established population of voids.

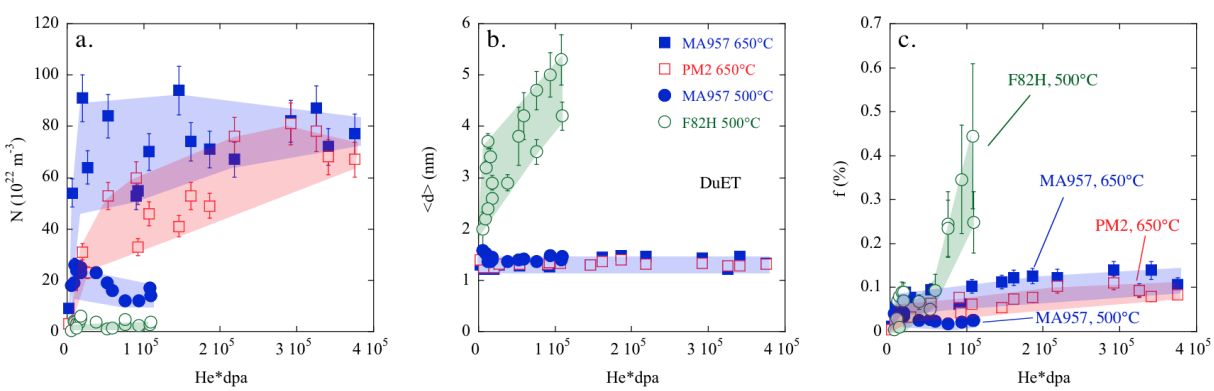

Figure 3. Comparison of all the dual ion beam irradiation results for N, <d> and f as a function of He*dpa.

ACKNOWLEDGEMENTS

The dual ion-beam irradiations were initially conducted in the TITAN program for US DOE-Japan MEXT collaboration for fusion energy research and continued under the support of the "Joint Research Program on Zero-Emission Energy Research," Institute of Advanced Energy, Kyoto University (ZE24A-13 and 23B-3). The work performed at UCSB was supported by the U. S. Department of Energy, Office of Fusion Energy Sciences, under contract DE-FG03-94ER54275. We acknowledge the contributions of the NSF sponsored UCSB Microstructure and Microanalysis Facility. We are also grateful for generous support of research materials, F82H mod.3 from Dr. K. Shiba, (JAEA, Japan), MA957 from Dr. R. J. Kurtz (PNNL) and 14YWT-PM2 from Dr. D. T. Hoelzer (ORNL).

REFERENCES

[1] Y. Dai, G. R. Odette, and T. Yamamoto, "The Effects of helium on irradiated structural alloys," *in Comprehensive Nuclear Materials,* R. Konings*,* T. R. Allen, R. E. Stoller, and S. Yamanaka, Eds. (2012) Elsevier.
[2] T. Yamamoto, G. R. Odette, L. R. Greenwood, Fusion Materials Semiannual Report 1/1 to 6/30/2005 DOE/ER-313/38 (2005) 95.
[3] T. Yamamoto, G. R. Odette, P. Miao, D. T. Hoelzer, J. Bentley, N. Hashimoto, H. Tanigawa, R. J. Kurtz, *J. Nucl. Mater*. **367-370** (2007) 399.
[4] R. J. Kurtz, G. R. Odette, T. Yamamoto, D. S. Gelles, P. Miao, and B. M. Oliver, *J. Nucl. Mater.* **367-370** (2007) 417.
[5] G. R. Odette, M. J. Alinger, and B. D.Wirth, Annu*. Rev. Mater. Res.* **38** (2008) 471.
[6] T. Yamamoto, G. R. Odette, P. Miao, D. J. Edwards, and R. J. Kurtz., *J. Nucl. Mater.* **386-388** (2009) 338.
[7] D. J. Edwards, R. J. Kurtz, G. R. Odette, and T. Yamamoto, *Fusion Materials Semiannual Report 12/31/2009* DOE/ER-313/47 (2010) 59.
[8] G. R. Odette, P. Miao, D. J. Edwards, T. Yamamoto, R. J. Kurtz, and Y. Tanigawa, *J. Nucl. Mater.* **417** (2011) 1001.
[9] E. H. Lee, J. D. Hunn, T. S. Byun and L. K. Mansur, *J.* Nucl. Mater. **280** (2000) 18.
[10] H. Kishimoto, K. Yutani, R. Kasada, and A. Kimura, *Fusion Eng. Des*. **81** (2006) 1045.
[11] R. Kasada, H. Takahashi, H. Kishimoto, K. Yutani, A. Kimura, *Mater. Sci. Forum* ***654-656*** (2010) 2791 (*doi:10.4028/www.scientific.net/MSF.654-656.2791).*
[12] T. Yamamoto, Y. Wu, G. R. Odette, K. Yabuchi, and A. Kimura, *Fusion Materials Semiannual Report 12/31/2010* DOE/ER-313/49 (2011) 1.
[13] K. Shiba, M. Enoeda, and S. Jitsukawa, *J. Nucl. Mater.* **329-333** (2004) 243.
[14] G. R. Odette and D. T. Hoelzer, *JOM* **62** (2010) 84.
[15] N. J. Cunningham, Y. Wu, G. R. Odette, D. T. Hoelzer, S. A. Maloy, Fusion Materials Semiannual Report 6/30/2013 DOE/ER-313/54 (2013) 15.
[16] N. J. Cunningham, Y. Wu, G. R. Odette, D. Gragg, K. Fields, D. T. Hoelzer, S. A. Maloy, Fusion Materials Semiannual Report 12/31/2012 DOE/ER-313/53 (2013) 20.
[17] M. L. Hamillton, D. S. Gelles, R. J. Lobsinger, M. M. Paxton, and W. F. Brown, "Fabrication Technology for ODS Alloy MA957," PNL-13165, Pacific Northwest Laboratory (2000).
[18] J. H. Kim, T. S. Byun, D. T. Hoelzer, S.-W. Kim, and B. H. Lee, *Mater. Sci. Eng. A* **559** (2013) 101.

[19] Y. Wu, E. M. Haney, N. J. Cunningham, and G. R. Odette, *Acta Meta.* **60** (2012) 3456.
[20] A. Kohyama, Y. Katoh, M. Ando, and K. Jimbo, *Fusion Eng. Des.* **51-52** (2000) 789.
[21] ASTM E521-96 (2009), ASTM
[22] R. E. Stoller, M. B. Toloczko, G. S. Was, A. G. Certain, S. Dwaraknath, and F. A. Garner, *Nucl. Instr. Methods Phys. Res. B* **310** (2013) 75.
[23] E. H. Lee, L. K. Mansur, and M. H. Yoo, *J. Nucl. Mater.* **85-86** (1979) 577.
[24] F. A. Garner, *J. Nucl. Mater.* **117** (1983) 177.
[25] A. D. Brailsford and L. K. Mansur, *J. Nucl. Mater.* **71** (1977) 110.
[26] R. E. Stoller and G. R. Odette, J. Nucl. Mater. **131** (1985) 118.
[27] W. A. Coughlan and L. K. Mansur, *J. Nucl. Mater.* **122-123** (1984) 495.
[28] F. A. Garner, M. B. Toloczko, and B. H. Sencer, *J. Nucl. Mater.* **276** (2000) 123.
[29] Y. Wu, T. Yamamoto, N. Cunningham, G. R. Odette, S. Kondo, and A. Kimura, Fusion Materials Semiannual Report 6/30/2013 DOE/ER-0313/54 (2013) 42.